# scientific reports

OPEN

# Preparation of MWCNT/CoMn$_2$O$_4$ nanocomposite for effectual degradation of picric acid via peroxymonosulfate activation

Ayda Farajollahi [ORCID] & Ahmad Poursattar Marjani [ORCID] [✉]

In recent years, using nanomaterials based on multi-wall carbon nanotubes (MWCNT) through the activation of peroxymonosulfate (PMS) has attracted more attention to the degradation of organic pollutants. This research presented a new route for the synthesis of MWCNT/CoMn$_2$O$_4$ nanocomposite for the degradation of picric acid using advanced oxidation processes (AOPs). Firstly, CoMn$_2$O$_4$ nanoparticles were prepared and then loaded on MWCNT using ultrasonic waves. The results of various analyzes confirmed the successful loading of nanoparticles on carbon nanotubes. As the degradation process proceeds through oxidation processes, the high electronic conductivity of MWCNT and the active sites of Mn and Co in the nanocomposite play an essential role in activating PMS to generate reactive oxygen species (ROS). An investigation of the reaction mechanism in different conditions showed that the highest speed of picric acid decomposition in the presence of nanocomposite (98%) was in 47 min. However, the scavenger test showed that HO$^.$ and SO$_4$$^{.-}$ radicals are more important in the degradation process. Meanwhile, the results showed that removing picric acid using MWCNT/CoMn$_2$O$_4$ was more effective than CoMn$_2$O$_4$ alone and confirmed the interaction effect of MWCNT nanotubes with AB$_2$O$_4$ nanocatalyst.

The rapid technological developments, the growing world population, and the increased diversification of industries have made the issue of supplying clean water one of the most challenging issues around[1]. Water is contaminated by different substances such as antibiotics, dyes, herbicides, etc., which severely threatens the health of humans, animals, and plants[2,3]. Dyes are one of the most critical water pollutants due to their use in various industries, such as leather, paper, and food[4,5]. Picric acid, or 2,4,6-trinitrophenol (TNP), is extensively employed in various industries such as pharmaceuticals, leather, explosives, chemicals, and dyes. Due to its high solubility in water, picric acid is one of the most significant water pollutants[6]. Due to the harmful effects of picric acid on the human body, especially the skin, kidneys, eyes, liver, and lungs, it is necessary to remove it from water[7].

Diverse methods have been reported for removing contamination from water, such as ozonation[8], photocatalytic treatment[9], degradation[10,11], adsorption/separation[12], and the Fenton process[13]. In recent years, the use of advanced oxidation procedures to remove pollutants from the water has received much attention[14–16]. Pollutants are removed using the progressive oxidation method by converting them into active radicals, such as sulfate (SO$_4$$^-$) and hydroxyl radicals ($^.$OH). The activation of persulfate and peroxymonosulfate (PMS), as well as covering peroxodisulfate (PDS), is one of the most effective sources for the production of SO$_4$$^{.-}$ radical[17].

However, we used PMS to degrade picric acid due to its availability, high activity, and cheapness. In recent decades, the spinel oxide AB$_2$O$_4$ (A/B = transition metal ions) catalysts and their composites have been utilized extensively because of their excellent synergistic effect between two kinds of metallic ions for removing water pollutants[18,19]. Using carbon nanotubes, due to their unique properties, such as high thermal conductivity and mechanical strength, as a substrate for the stabilization and stability of nanoparticles has received much attention from researchers[20,21]. Many reports have been presented in the field fabrication of CoMn$_2$O$_4$ nanoparticles based on various carbon materials, including pg-C$_3$N$_4$/CoMn$_2$O$_4$[22], CoMn$_2$O$_4$@N-rGA[23], CoMn$_2$O$_4$/NC[24], and CoMn$_2$O$_4$/C hollow spheres[25]. Our findings show that no research has been reported on utilizing MWCNT/

Department of Organic Chemistry, Faculty of Chemistry, Urmia University, Urmia, Iran. [✉]email: a.poursattar@urmia.ac.ir

$CoMn_2O_4$ nanostructure in the removal reaction of picric acid through activation PMS. In this study, the prepared nanocomposite performed excellently in activating PMS for the degradation of picric acid as an organic contamination. The combination of cobalt and manganese nanoparticles with carbon nanotubes is due to the high activity in removing pollutants and electron transfer on carbon nanotubes. This research proposes an easy and new method for preparing of MWCNT/$CoMn_2O_4$ nanocomposite. Also, the synergistic effect $CoMn_2O_4$ of nanoparticles on multi-walled carbon nanotubes for the degradation of picric acid via the activation of peroxymonosulfate was investigated. Evaluation of picric acid degradation reaction using MWCNT/$CoMn_2O_4$ of nanocomposite in different conditions obtained good results. As far as we know, the economic preparation of nanocomposite that can activate peroxymonosulfate for the degradation of picric acid has not been presented.

## Experimental

### Chemicals
Multi-wall carbon nanotube (MWCNT), cobalt(II) chloride, manganese(II) acetate, oxalic acid, sodium hydroxide (NaOH), benzoquinone (BQ), ethanol (EtOH), potassium dichromate ($K_2Cr_2O_7$), sodium azide ($NaN_3$), and isopropyl alcohol (IPA) were procured from Sigma-Aldrich, )Germany( and Merck (Germany). Distilled water and ethanol were used as solvents in all processes. Meantime, picric acid (96% purity) was procured from Alvan Sabet Company (Iran).

### Instrumentation
Infrared spectra were obtained utilizing a (Shimadzu IR-640 spectrometer, Japan). XRD diffraction patterns were identified with a (Philips-PW 1730, Germany). Field Emission Scanning Electron Microscope (FE-SEM) and sample mapping were prepared using a (TESCAN MIRA3 microscope, Czech Republic). Transmission electron microscopy (TEM) was recorded using (Philips EM 208S, Netherlands). The images of the surface roughness of the nanostructure were obtained using the Atomic Force Microscope (AFM, Brisk, Germany). X-ray Photoelectron Spectroscopy (XPS, EA 10 analysis system, Germany) determined the type of bonds and chemical composition. The electronic vibrations of the nanocomposite and the degradation efficiency were investigated with (Labmann LMSP UV-1200, Canada).

### Fabrication of $CoMn_2O_4$ nanoparticles
The $CoMn_2O_4$ nanoparticles were fabricated in conformity with Wang et al.'s report with a few corrections[22]. To form a pure solution, 1.74 g of $Mn(CH_3CO_2)_2$ and 650 mg of $CoCl_2$ were dissolved in a mixture of water–ethanol with a ratio (1:1). Then, 1 g of oxalic acid was added to the medium reaction under vigorous stirring. After a while, to adjust the pH of the solution to 7 that 1 M of sodium hydroxide was used slowly dropwise, and the resulting solution was stirred at 80 °C for 10 h. After cooling down naturally, the black color as prepared was filtered, rinsed many times with ethanol/water, and dried at 80 °C. Eventually, the compound prepared was calcined for 3 h at 500 °C.

### Fabrication of MWCNT/$CoMn_2O_4$ nanocomposite
In the fabrication of this nanocomposite, 20 mg of MWCNT was added in 10 mL of ethanol to prepare a suspension solution via sonication for 60 min (Fig. 1). Then, 20 mg of as-obtained $CoMn_2O_4$ was added to the reaction
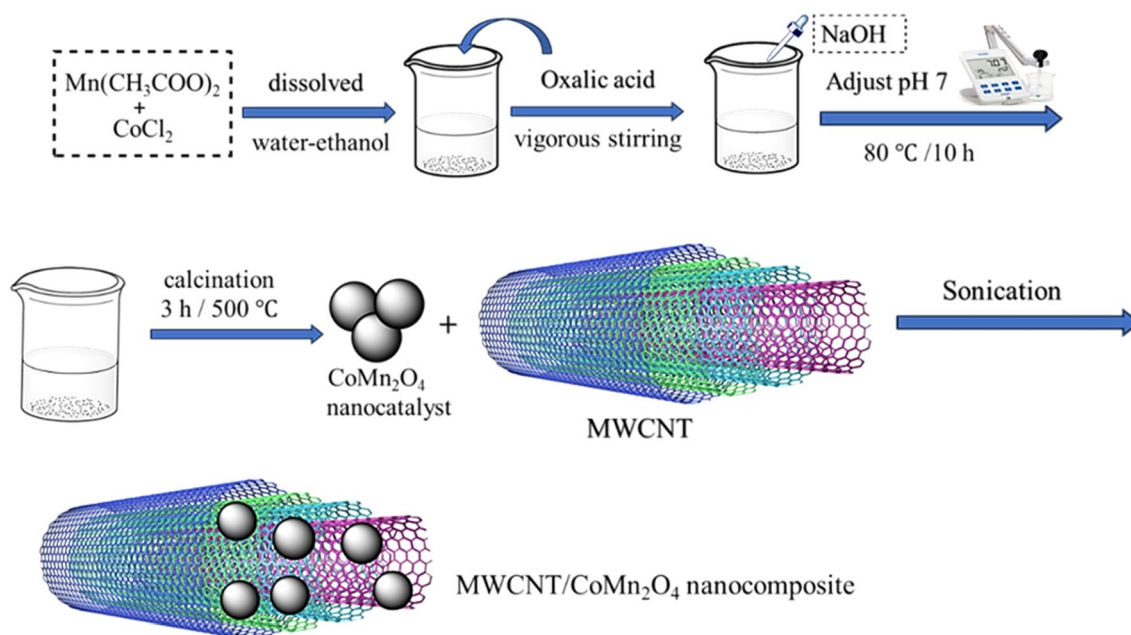


**Figure 1.** Synthetic approach for the synthesis of MWCNT/$CoMn_2O_4$ nanocomposite.

mixture and sonicated (30 min) to significant adsorption of $CoMn_2O_4$ nanoparticles on the multi-wall carbon nanotubes. Next, the process admixture was often filtered and rinsed with ethanol/water. Eventually, it was dried at 80 °C for 12 h to produce MWCNT/$CoMn_2O_4$ nanocomposite[26].

## Degradation test

The degradation process of picric acid was investigated in the presence of various dosages of MWCNT/$CoMn_2O_4$ nanocomposite as a PMS activator. The removal reaction of picric acid was checked under different conditions and using various nanocomposite dosages as a PMS activator. In the optimum condition, the removal reaction of picric acid by adding 0.05 g/L MWCNT/$CoMn_2O_4$ was put into 100 mL of picric acid solution (10 mg/L) in 30 min until it reached the adsorption–desorption equilibrium. After a while, to generate reactive species oxygen (ROS), PMS (0.3 g/L) was added to the primal process admixture. In the end, the degradation reaction was investigated via a UV–Vis spectrophotometer. The prominent absorbance peak of picric acid was observed at 354 nm, and due to the following relation, the removal efficiency was calculated:

$$\text{Removal efficiency (\%)} = \frac{C_t - C_o}{C_o} \times 100$$

$C_o$ and $C_t$ are the final and initial picric acid concentrations, respectively.

## Results and discussion

In addition to the scientific findings in developing nanoparticles to degrade organic pollutants[27–31], in the present research, a new strategy for the preparation of MWCNT/$CoMn_2O_4$ nanocomposite for the degradation of picric acid through the activation of peroxymonosulfate has been presented. The strategy of MWCNT/$CoMn_2O_4$ of nanocomposite synthesis consists of 2 steps, in which $CoMn_2O_4$ nanoparticles were prepared in step 1. In step 2, for the synthesis of MWCNT/$CoMn_2O_4$ nanocomposite, $CoMn_2O_4$ nanoparticles prepared using ultrasonic waves were placed on the walls of carbon nanotubes. The unique properties of carbon nanotubes have caused changes in the performance of nanoparticles and increased catalytic power. Therefore, the performance of the synthesized nanocomposite was evaluated in the process of picric acid degradation as an organic pollutant through peroxymonosulfate activation. In comparing this nanocomposite with other nanocomposites[32–36], we can point out its distinctive features such as easy preparation, short degradation time, structural checking via various analyses, especially XPS and AFM spectrum, high degradation efficiency, excellent performance by few dosages of the nanocomposite in the degradation process, degradation with the easy method without the need to sunlight and radiation, and investigating the removal picric acid as a vital contamination in drug and industries.

## Characterization

The X-ray diffraction pattern has been used to identify and distinguish the crystal structure and crystal size of the synthesized $CoMn_2O_4$ nanocatalyst and MWCNT/$CoMn_2O_4$ nanocomposite. As shown in Fig. 2b, the different peaks emerged in 18.67°, 29.37°, 31.57°, 33.32°, 44.82°, 61.12°, and 65.53° were related to (102), (110), (202), (213), (222), (225), and (402) in $CoMn_2O_4$ nanoparticles surfaces (JCPDS No. 29-1487), respectively. Among various peaks, 36.72°(104) was obtained, corresponding to the $CoMn_2O_4$ nanocatalyst[37]. In addition, a peak at 26.78° can belong to multi-wall nanocarbon nanotubes[38]. Based on the findings from XRD patterns, both $CoMn_2O_4$ and MWCNT/$CoMn_2O_4$ nanocomposites were successfully prepared.

The FT-IR spectrum was investigated to find the functional groups in $CoMn_2O_4$ and MWCNT/$CoMn_2O_4$ nanocomposite from 400 to 4000 cm$^{-1}$. As indicated in Fig. 2a, a strong peak near 3445 cm$^{-1}$ corresponding to O–H stretching appeared due to the absorption of $H_2O$ on the nanocomposite surface. However, there are various peaks at 1126, 1390, 1627, and 2930 cm$^{-1}$, which were related to C–C, C–O, C=O, and C–H, respectively. MWCNT/$CoMn_2O_4$ nanocomposite has two peaks at 626 and 543 cm$^{-1}$ because of Co–O and Mn–O bonds,



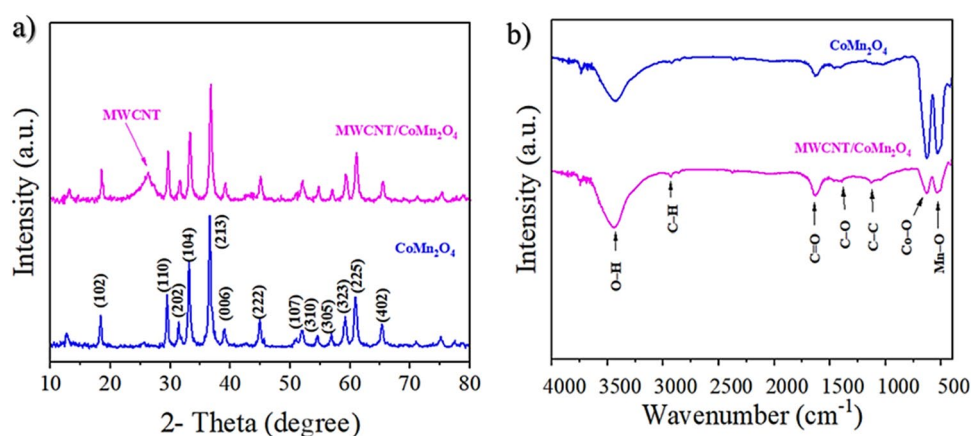**Figure 2.** XRD (**a**) and FT-IR (**b**) pattern of $CoMn_2O_4$ and MWCNT/$CoMn_2O_4$ nanostructures.

respectively[39,40]. Based on the peaks in the nanoparticle and nanocomposite structure (related to each of the functional groups) that are characteristic of the pure and correct form of the products after synthesis, it may be concluded that the compounds were produced adequately.

The electronic states and elemental composition of the $CoMn_2O_4$ and $MWCNT/CoMn_2O_4$ nanostructure were assessed by XPS, as shown in Fig. 3. The full scan XPS spectrum of the nanostructure (Fig. 3a) displayed the existence of elements C, Co, Mn, and O in the $CoMn_2O_4$ and $MWCNT/CoMn_2O_4$ nanostructure. The high-resolution spectrum of C 1s is divided into four peaks (Fig. 3b), which involving energy bands of 291.40 eV are related to the 284.7 eV to the C=C bond 285.3 eV to the C–C bond, 286.3 eV to the C–O bond, and 287.7 eV to the C=O bond. Figure 3c indicates the high-resolution XPS spectrum of Co 2p. The Co atom was demonstrated in two oxidation states, $Co^{+2}$ and $Co^{+3}$, in the structure of the $MWCNT/CoMn_2O_4$ compound. Two peaks correspond to Co 2p1/2 and Co 2p3/2. The peak at 932.15 eV is assigned to $Co^{2+}$, while two peaks at 936.4 and 954.17 eV can attributed to $Co^{3+}$. Peaks at 529.7, 531.5, and 533.6 eV in the O 1s XPS spectra (Fig. 3d) can be linked to hydroxyl groups, metal–oxygen bonds, and absorbed water, respectively. High-resolution XPS spectrum of Mn appeared in $Mn^{2+}$, $Mn^{3+}$, and $Mn^{4+}$ oxidation states (Fig. 3e). The peak related to $Mn^{2+}$ appeared at 640.6, while the two peaks linked to $Mn^{3+}$ were revealed at 642.2 and 653.4 eV. In addition, peaks belonging to $Mn^{4+}$ were observed at 644.2 and 655 eV.

FESEM, TEM, and AFM investigated the structure and surface morphology of $CoMn_2O_4$ and $MWCNT/CoMn_2O_4$ nanocomposite. As displayed in Fig. 4a, the $CoMn_2O_4$ nanoparticles have a symmetrical geometry morphology with cuboid microcrystals. Also, the thickness of nanoparticles was evaluated between 0.1 and 1 μm. Meanwhile, the MWCNT appeared in tubular morphology, corroborating the loading of $CoMn_2O_4$ nanostructures on the MWCNT (Fig. 4b). Elemental distribution maps and EDX spectra were utilized to measure the elements' distribution, and nanocomposite purity. Both analyses' results acknowledged the high purity of carbon, cobalt, manganese, and oxygen elements in the nanocomposite structure (Fig. 4c). The result obtained from elemental mapping analysis is exhibited in Fig. 4d.

An atomic force microscope (AFM) is an essential and helpful instrument for checking the topography of the surface on a nanometer scale. This microscope is used to image the roughness of the nanostructure surface and provide two- and three-dimensional images. The results obtained from the AFM analysis of the nanocomposite structure are indicated in Fig. 5. As shown in Fig. 5, the $CoMn_2O_4$ nanoparticles have mountain-like morphology with white edges. In contrast, MWCNT has a non-intersecting surface on which $CoMn_2O_4$ nanoparticles were placed. In the meantime, the surface roughness of the $MWCNT/COMn_2O_4$ nanocomposite was estimated at 25.62 nm.

TEM is applied to clarify the structure and the morphology of $MWCNT/CoMn_2O_4$ nanocomposite even more. The results of the images can be seen in the Fig. 6. These images depict nanoparticles correctly placed on multi-wall carbon nanotubes with high magnification. $CoMn_2O_4$ nanoparticles are loaded in black aggregates similar to those between the walls of carbon nanotubes. Compared to SEM, the TEM analysis gives a detailed look at the nanocomposite.
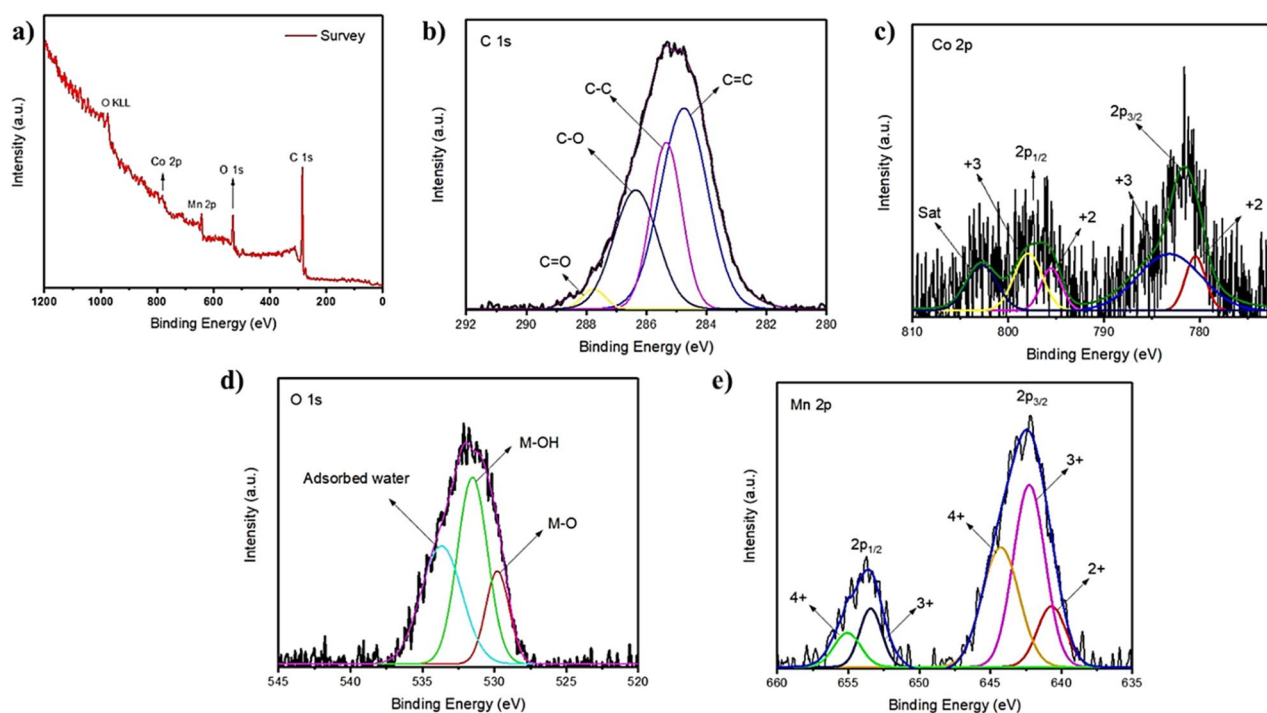


**Figure 3.** XPS spectra of the $MWCNT/CoMn_2O_4$ nanostructure: survey scan (**a**), C 1s (**b**), Co 2p (**c**), O 1s (**d**), and Mn 2p (**e**).
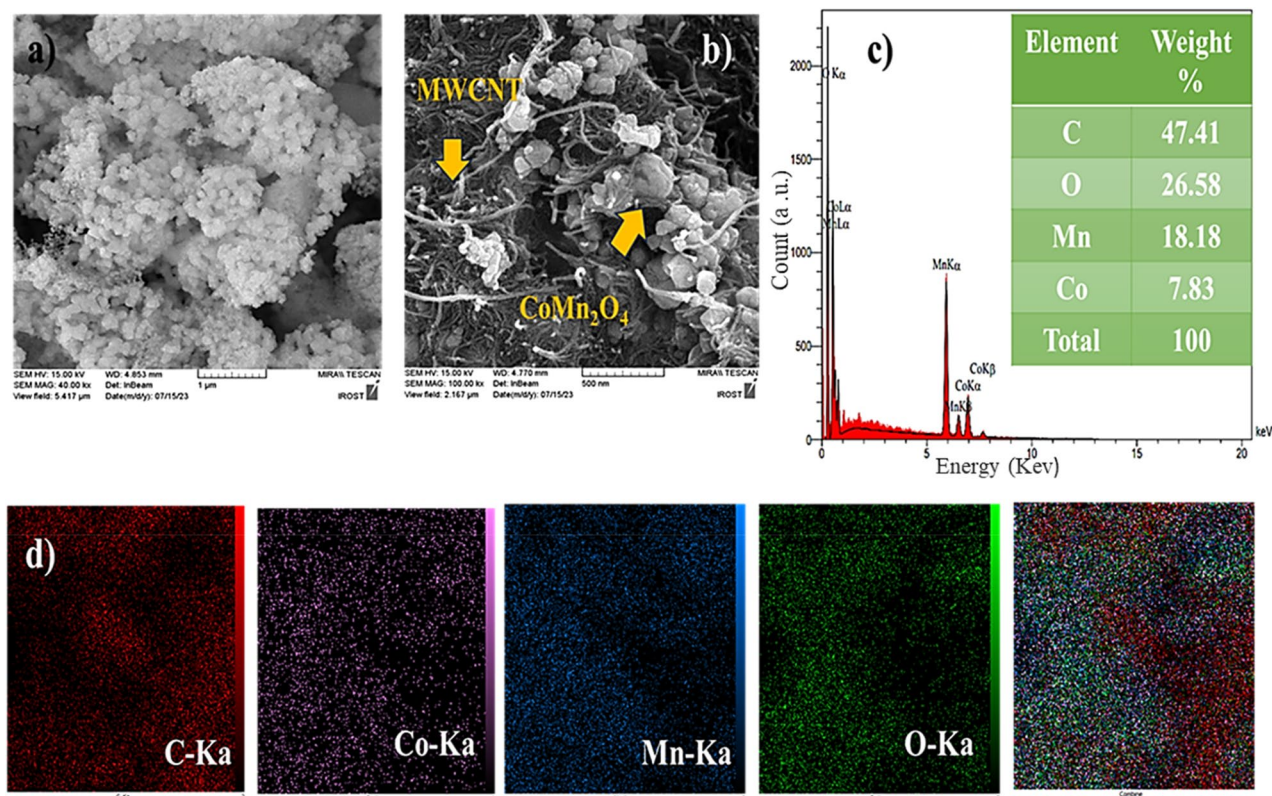
**Figure 4.** FESEM images CoMn$_2$O$_4$ (**a**), MWCNT/ CoMn$_2$O$_4$ (**b**), EDX (**c**), and SEM-mapping (**d**) of the nanocomposite.
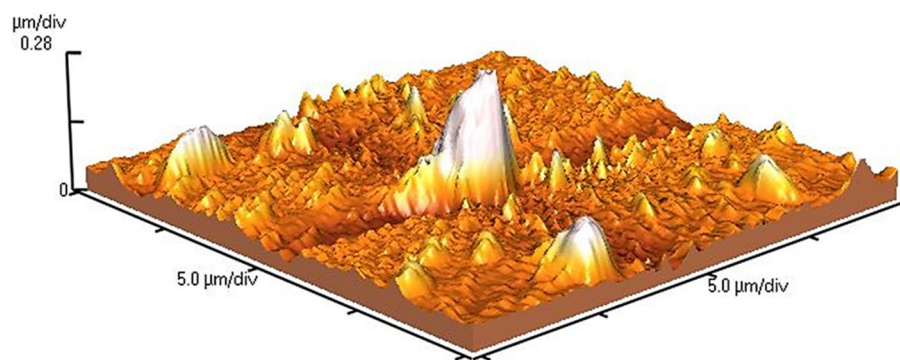


**Figure 5.** AFM image of MWCNT/CoMn$_2$O$_4$.

## Degradation efficiency

Due to the severe water scarcity in many places, the destruction of organic pollutants, particularly picric acid, which is detrimental to the human body, animals, and plants, has come to notice. Hence, MWCNT/CoMn$_2$O$_4$ nanocomposite, which is totally synthesized and characterized afterward, is employed in this study to act as the PMS activator to degrade picric acid efficiently. The efficiency of the nanocomposite in the production of picric acid hydrolysis was determined by performing the test in the presence of various factors, and the results are shown in Fig. 7. The consequences displayed that utilization of the CoMn$_2$O$_4$ caused degradation of picric acid with yield degradation of 24% within 120 min. Without PMS, MWCNT/CoMn$_2$O$_4$ nanocomposite can only remove about 12% of picric acid in 80 min. The reaction of the picric acid degradation using both PMS (0.3 g/L) and MWCNT/CoMn$_2$O$_4$ nanocomposite (0.05 g/L) went well as expected. Also, the degradation of the picric acid takes place within 47 min. In the degradation of picric acid from wastewater, the offered nanocomposite can compete with the other nanocomposites (Table 1).
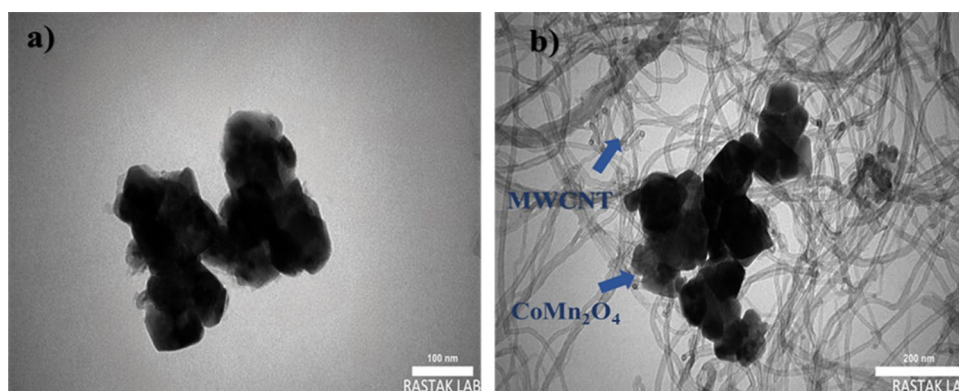
**Figure 6.** TEM images of CoMn$_2$O$_4$ (**a**) and MWCNT/CoMn$_2$O$_4$ nanostructures (**b**).
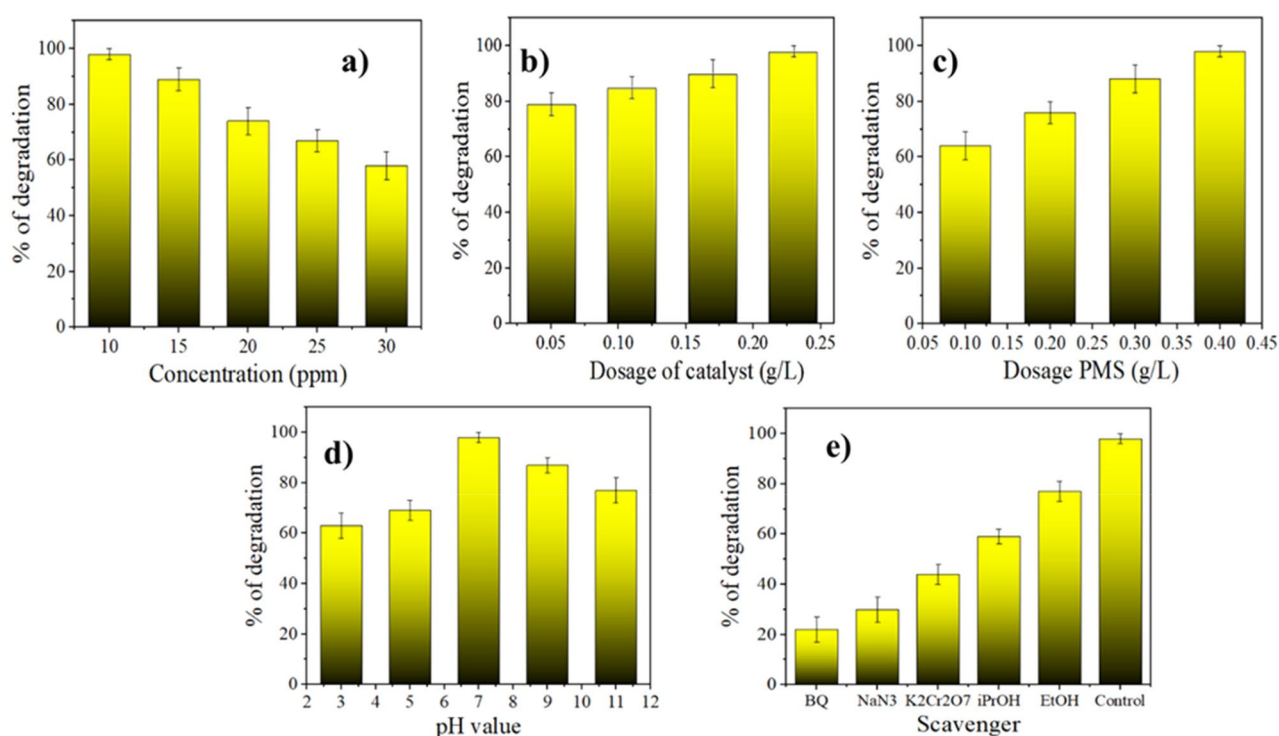


**Figure 7.** Impact of various factories in % of remove: the concentration of CV (**a**), a dosage of catalyst (**b**), the dosage of PMS (**c**), pH (**d**), and scavenger (**e**).

| Nanocomposites | Treatment | Efficiency (%) | Process conditions | References |
|---|---|---|---|---|
| rGO-TiO$_2$ | H$_2$O$_2$ | 100 | [C$_{PA}$] = 200 ppm, [cat] = 50 mg/L, [H$_2$O$_2$] = 50 mg/L, 15 min | 37 |
| Nano-CeO$_2$-loaded chitosan-bocglycine zinc complex | H$_2$O$_2$ | 100 | [C$_{PA}$] = 200 ppm, [cat] = 50 mg/L, [H$_2$O$_2$] = 20 mM/L, 35 min | 38 |
| Pd@TiO$_2$ | Catalyst | 100 | [C$_{PA}$] = 500 ppm, [cat] = 20 mg/L, 70 min | 39 |
| Ag/ZnO | Photocatalyst | 90 | [C$_{PA}$] = 10 ppm, [cat] = 60 mg/L, 150 min | 40 |
| MWCNT-Chi | Catalyst | 90 | [C$_{PA}$] = 100 ppm, [cat] = 20 mg/L, 240 min | 41 |
| AV-TiO$_2$ | Photocatalyst | 97 | [C$_{PA}$] = 500 ppm, [cat] = 20 mg/L, 120 min | 42 |
| **MWCNT/CoMn$_2$O$_4$** | **PMS** | **98** | **[C$_{PA}$] = 10 ppm, [cat] = 0.05 g/L, [PMS] = 0.3 g/L, 47 min** | **Current work** |

**Table 1.** The studies of picric acid removal with the utilization of different nanocomposites. Significant values in bold.

## Impact of various factors

The effect of picric acid concentration was investigated from 10 to 30 ppm in the picric acid degradation, and the degradation yield of picric acid reduced from 98 to 58% (Fig. 7a). This can be related to the saturation of reactive levels in the nanocomposite, which reduces ROS. Also, the effect of the MWCNT/CoMn$_2$O$_4$ nanocomposite dosage was measured in dosages of 0.05, 0.1, 0.15, and 0.2 g/L in the picric acid removal. As indicated in Fig. 7b, because of efficient nanoparticles of cobalt, manganese and the high electrical conductivity of carbon nanotubes on the level of the nanocomposite, the picric acid removal increased between 79 and 98% within 47 min. Nonetheless, the degradation process of picric acid was evaluated at PMS concentrations of 0.1, 0.2, 0.3, and 0.4 g/L, and picric acid removal was enhanced from 64 to 98% (Fig. 7c). The good impact of this factor is because of the delivery of reactive oxygen species, including HO$^{\cdot}$, O$_2$$^{\cdot-}$, $^1$O$_2$, and SO$_4$$^{\cdot-}$. The degradation reactions of picric acid using MWCNT/CoMn$_2$O$_4$ nanostructure at different pHs from 3 to 10 were studied and displayed in Fig. 7d. The findings acquired from the impact of pH on the removal reactions specified that the removal of picric acid occurred more successfully in alkaline than in acidic pH. After that, the scavenger experiment was utilized to investigate the radical species included in the removal reaction. We conducted studies on the removal reaction of picric acid by use of various scavengers such as sodium azide (NaN$_3$), ethanol, benzoquinone (BQ), isopropyl alcohol (IPA), and potassium dichromate (K$_2$Cr$_2$O$_7$). According to Fig. 7e, the species HO$^{\cdot}$ and SO$_4$$^{\cdot-}$ are mostly noticed as the significant radicals in degradation reactions, and the catalytic performance must be a low weaken using of EtOH for scavenging HO$^{\cdot}$ and SO$_4$$^{\cdot-}$. As provided in Fig. 7e, when EtOH was used as a scavenger, the picric acid degraded by efficacy 77% after 47 min. In conjunction with it, the yield removal of picric acid using IPA was 59%. In conformity with the finding, it was determined that EtOH and IPA have an excellent scavenging action compared to sulfate and hydroxyl species. To check the activity of nanostructure for practical applications in the removal reaction, we performed the process on a large scale. For this reason, we utilized picric acid (10 mg/L) of MWCNT/CoMn$_2$O$_4$ nanostructure (0.05 g/L) and PMS (0.3 g/L) to carry out the removal reaction on a larger scale, which caused a more effective remove of picric acid in 47 min. The outcomes indicated that this process is practically stable and manageable.

## Proffered mechanism of picric acid removal

Based on the findings, a possible mechanism was presented for the degradation of picric acid via radicals and electron transforms (Fig. 8). The results indicated that placing CoMn$_2$O$_4$ nanoparticles onto the multi-wall carbon nanotubes caused an increase in transform electron and degradation yield. Meanwhile, there are many methods for producing free radicals, including ozone, hydrogen peroxide, and persulfate[41]. In this study, MWCNT/CoMn$_2$O$_4$ nanocomposite removed the organic pollutant by using PMS to produce $^{\cdot}$OH, SO$_4$$^{\cdot-}$, $^1$O$_2$, and O$_2$$^{\cdot-}$ prepared radicals. However, the SO$_4$$^{\cdot-}$ radical reacts highly with organic contaminations because of its excellent oxidative potential[42]. Also, the scavenging test was utilized to show the roles of ROS in the degradation reaction. In the removal process, different scavengers, such as sodium azide (NaN$_3$), potassium dichromate (K$_2$Cr$_2$O$_7$), isopropyl alcohol ($^i$PrOH), ethanol (EtOH), and benzoquinone (BQ), have been checked to trap radicals. According to the findings, the degradation process happened with a higher yield in ethanol than in the presence of other scavengers. The prominent radicals in the reaction are OH$^{\cdot}$ and SO$_4$$^{\cdot-}$ due to the ethanol being a trapper of
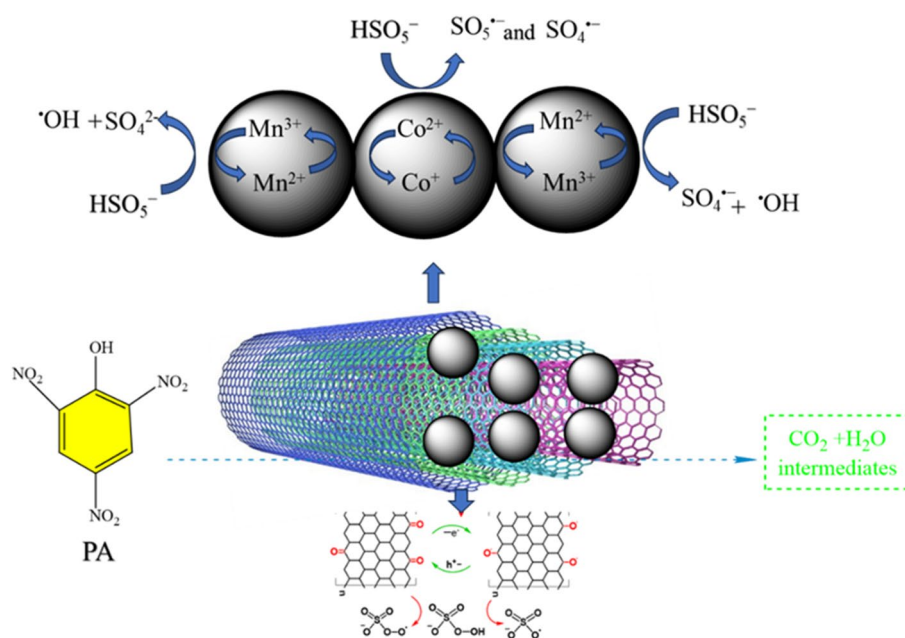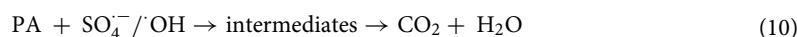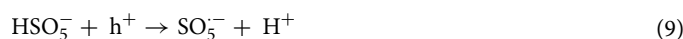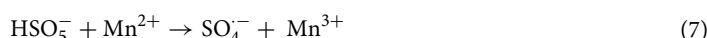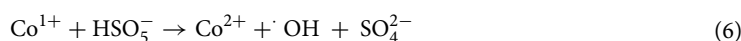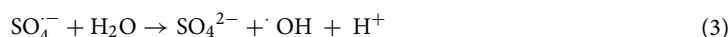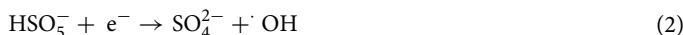


**Figure 8.** The mechanism for PA removal was presented using the MWCNT/CoMn$_2$O$_4$ through the activation of PMS.

OH$^.$ and SO$_4$$^{.-}$. The manganese and cobalt on the surface of MWCNT were reacted by PMS (HSO$_5$$^-$) to generate SO$_4$$^{.-}$ and $^.$OH with Eqs. (1) and (2)[43]. Then, to create $^.$OH, water was reacted with SO$_4$$^{.-}$ radicals (Eq. 3). In the next step, the Co$^+$ ion and SO$_5$$^{.-}$ radical were prepared for the reaction of Co$^{2+}$ ions on the surface MWCNT/CoMn$_2$O$_4$ by PMS (Eq. 4). Since the Co$^{1+}$ ion converted to Co$^{2+}$ (Eq. 5). Meantime, Co$^{2+}$, SO$_4$$^{2-}$, and OH$^.$ were prepared from the reaction Co$^{1+}$ ions with HSO$_5$$^-$ (Eq. 6)[44]. Respectively, the SO$_4$$^{.-}$ and SO$_5$$^{.-}$ were prepared from the reaction of the Mn$^{2+}$ and Mn$^{3+}$ ions on the surface MWCNT/CoMn$_2$O$_4$ with HSO$_5$$^-$ (Eqs. 7 and 8)[45]. However, multi-wall carbon nanotubes can have an essential obligation in electron transfer to PMS because of their distinctive properties (Eq. 9). In the end, to complete the degradation process of organic contaminant, the OH$^.$ and SO$_4$$^{.-}$ radicals with the picric acid were turned into H$_2$O, CO$_2$, and intermediate (Eq. 10).

$$HSO_5^- + e^- \rightarrow SO_4^{.-} + {}^.OH \tag{1}$$

$$HSO_5^- + e^- \rightarrow SO_4^{2-} + {}^.OH \tag{2}$$

$$SO_4^{.-} + H_2O \rightarrow SO_4^{2-} + {}^.OH + H^+ \tag{3}$$

$$Co^{2+} + HSO_5^- \rightarrow Co^{2+} + SO_5^{.-} \tag{4}$$

$$Co^{1+} + HSO_5^- \rightarrow Co^{2+} + SO_4^{.-} \tag{5}$$

$$Co^{1+} + HSO_5^- \rightarrow Co^{2+} + {}^.OH + SO_4^{2-} \tag{6}$$

$$HSO_5^- + Mn^{2+} \rightarrow SO_4^{.-} + Mn^{3+} \tag{7}$$

$$HSO_5^- + Mn^{3+} \rightarrow SO_5^{.-} + Mn^{2+} \tag{8}$$

$$HSO_5^- + h^+ \rightarrow SO_5^{.-} + H^+ \tag{9}$$

$$PA + SO_4^{.-}/{}^.OH \rightarrow intermediates \rightarrow CO_2 + H_2O \tag{10}$$
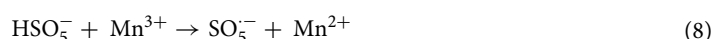
## Reusability investigations

Compared to previous works, one of the distinguishing features of this work is the ability to reuse the nanocomposite during several cycles. In this research, to investigate the reusability of the nanocomposite after performing the desired reaction, we separated the nanocomposite via a centrifuge (2800 rpm for 15 min) from the reaction mixture, several times rinsed with water/ethanol and next dried it at 100 °C during 7 h. According to Fig. 9, the MWCNT/CoMn$_2$O$_4$ nanocomposite was recycled during four cycles, and no significant change in its activity was observed during the recycling process. Also, the structure of the recycled nanocomposite was studied through different analyses, such as FESEM (Fig. 9b) and TEM (Fig. 9c). Investigations showed that its structure remained almost constant.

## Conclusions

In this research, a new generation of MWCNT/CoMn$_2$O$_4$ nanocomposite was designed and successfully made to degrade picric acid. The results obtained through different analyzes confirmed the growth and stabilization of CoMn$_2$O$_4$ nanoparticles on MWCNT. The presence of cobalt and manganese active sites on nanoparticles and the
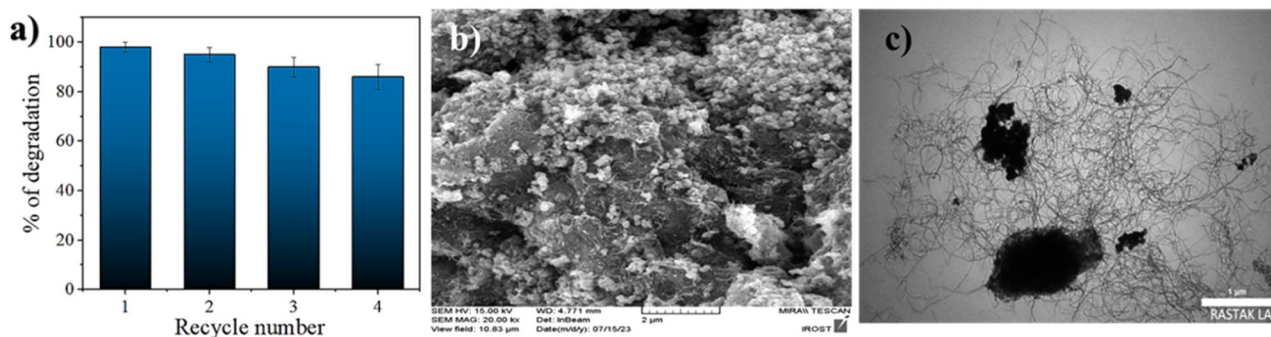


**Figure 9.** Results of recycling MWCNT/CoMn$_2$O$_4$ nanocomposite for PA remove reaction (**a**), FESEM (**b**), and TEM (**c**) images of the MWCNT/CoMn$_2$O$_4$ after 4th recycle reaction.

growth of CoMn$_2$O$_4$ nanoparticles on MWCNT as a substrate showed a significant increase in catalytic activity towards the degradation of picric acid. In addition, the investigation of the reaction mechanism and various tests, especially the scavenger test, confirmed that SO$_4$$^{-}$ and ·OH radicals play an essential role in the degradation of picric acid. Finally, the current study provides new insight into designing and fabricating nanoparticles on carbon nanotubes to improve water treatment.

## Data availability
All data have been given in the article.

## References
1. Shang, Y., Xu, X., Gao, B., Wang, S. & Duan, X. Single-atom catalysis in advanced oxidation processes for environmental remediation. *Chem. Soc. Rev.* **50**, 5281–5322 (2021).
2. Alharbi, O. M., Khattab, R. A. & Ali, I. Health and environmental effects of persistent organic pollutants. *J. Mol. Liq.* **263**, 442–453 (2018).
3. Balkanloo, P. G., Sharifi, K. M. & Poursattar Marjani, A. Graphene quantum dots: Synthesis, characterization, and application in wastewater treatment: A review. *Mater. Adv.* **4**, 4272–4293 (2023).
4. Xin, Z. *et al.* Novel nanozyme Ag/Fe$_3$O$_4$@h-BN with peroxidase-mimicking and oxidase-mimicking activities for dye degradation, As(V) removal and detection. *Chem. Eng. J.* **461**, 141589 (2023).
5. Sarreshtehdar Aslaheh, H., Poursattar Marjani, A. & Gozali Balkanloo, P. Pelargonium as a cost-effective additive in bio-composite adsorbent in removing dyes from wastewater: Equilibrium, kinetic, and thermodynamic studies. *J. Polym. Environ.* **31**, 3230–3247 (2023).
6. Hussain, S., Malik, A. H., Afroz, M. A. & Iyer, P. K. Ultrasensitive detection of nitroexplosive-picric acid via a conjugated polyelectrolyte in aqueous media and solid support. *Chem. Commun.* **51**, 7207–7210 (2015).
7. Kumar, R. *et al.* Fe-doped ZnO nanoellipsoids for enhanced photocatalytic and highly sensitive and selective picric acid sensor. *Mater. Res. Bull.* **102**, 282–288 (2018).
8. Hassani, A., Khataee, A., Fathinia, M. & Karaca, S. Photocatalytic ozonation of ciprofloxacin from aqueous solution using TiO$_2$/MMT nanocomposite: Nonlinear modeling and optimization of the process via artificial neural network integrated genetic algorithm. *Process. Saf. Environ. Protect.* **116**, 365–376 (2018).
9. Alamgholiloo, H. *et al.* Facile fabrication of Z-scheme TiO$_2$/ZnO@MCM-41 heterojunctions nanostructures for photodegradation and bioactivity performance. *J. Mol. Liq.* **364**, 119990 (2022).
10. Matzek, L. W., Tipton, M. J., Farmer, A. T., Steen, A. D. & Carter, K. E. Understanding electrochemically activated persulfate and its application to ciprofloxacin abatement. *Environ. Sci. Technol.* **52**, 5875–5883 (2018).
11. Farajollahi, A., Poursattar Marjani, A., Noroozi Pesyan, N. & Alamgholiloo, H. Efficient degradation of crystal violet by GO/CuMn$_2$O$_4$ nanocomposite via peroxymonosulfate activation. *Appl. Surf. Sci.* **622**, 156903 (2023).
12. Konwar, A., Gogoi, A. & Chowdhury, D. Magnetic alginate-Fe$_3$O$_4$ hydrogel fiber capable of ciprofloxacin hydrochloride adsorption/separation in aqueous solution. *RSC Adv.* **5**, 81573–81582 (2015).
13. Shoorangiz, M., Nikoo, M. R., Salari, M., Rakhshandehroo, G. R. & Sadegh, M. Optimized electro-Fenton process with sacrificial stainless steel anode for degradation/mineralization of ciprofloxacin. *Process. Saf. Environ. Protect.* **132**, 340–350 (2019).
14. Liu, Y. & Wang, J. Multivalent metal catalysts in Fenton/Fenton-like oxidation system: A critical review. *Chem. Eng. J.* **466**, 143147 (2023).
15. Liu, Y., Zhao, Y. & Wang, J. Fenton/Fenton-like processes with in-situ production of hydrogen peroxide/hydroxyl radical for degradation of emerging contaminants: Advances and prospects. *J. Hazard. Mater.* **404**, 124191 (2021).
16. Wang, J. & Zhuan, R. Degradation of antibiotics by advanced oxidation processes: An overview. *Sci. Total Environ.* **701**, 135023 (2020).
17. Wang, J. & Wang, S. Activation of persulfate (PS) and peroxymonosulfate (PMS) and application for the degradation of emerging contaminants. *Chem. Eng. J.* **334**, 1502–1517 (2018).
18. Zhao, L., Yang, D., Ma, L., Feng, X. & Ding, H. An efficient heterogeneous catalyst of FeCo$_2$O$_4$/g-C$_3$N$_4$ composite for catalytic peroxymonosulfate oxidation of organic pollutants under visible light. *Colloids Surf. A Physicochem. Eng. Asp.* **610**, 125725 (2021).
19. Qiu, S., Gou, L., Cheng, F., Zhang, M. & Guo, M. An efficient and low-cost magnetic heterogenous Fenton-like catalyst for degrading antibiotics in wastewater: Mechanism, pathway and stability. *J. Environ. Manag.* **302**, 114119 (2022).
20. Shoukat, R. & Khan, M. I. Carbon nanotubes: A review on properties, synthesis methods and applications in micro and nanotechnology. *Microsyst. Technol.* **27**, 4183–4192 (2021).
21. Chen, C., Ali, A., Toufouki, S., Jiang, W. & Yao, S. A hybrid electro-driven adsorption and degradation system for antibiotics and dyes based on composite tablets composed of deep eutectic solvent-functionalized nanomaterials. *Chem. Eng. J.* **471**, 144776 (2023).
22. Wang, Y., Nie, Z., Li, X., Zhao, Y. & Wang, H. Highly sensitive and selective electrochemical sensor based on porous graphitic carbon nitride/CoMn$_2$O$_4$ nanocomposite toward heavy metal ions. *Sens. Actuators B Chem.* **346**, 130539 (2021).
23. Ren, F. *et al.* CoMn$_2$O$_4$ nanoparticles embed in graphene oxide aerogel with three-dimensional network for practical application prospects of oxytetracycline degradation. *Sep. Purif. Technol.* **259**, 118179 (2021).
24. Ho, J. *et al.* Ionothermal synthesis of N-doped carbon supported CoMn$_2$O$_4$ nanoparticles as ORR catalyst in direct glucose alkaline fuel cell. *Int. J. Hydrogen Energy* **46**, 20503–20515 (2021).
25. Ma, Y. *et al.* Sandwich-shell structured CoMn$_2$O$_4$/C hollow nanospheres for performance-enhanced sodium-ion hybrid supercapacitor. *Adv. Energy Mater.* **12**, 2103820 (2022).
26. Katowah, D. F. *et al.* Selective fabrication of an electrochemical sensor for Pb$^{2+}$ based on poly (pyrrole-*co-o*-toluidine)/CoFe$_2$O$_4$ nanocomposites. *ChemistrySelect* **4**, 10609–10619 (2019).
27. Mohammed Mohammed, H. A. *et al.* A novel biosynthesis of MgO/PEG nanocomposite for organic pollutant removal from aqueous solutions under sunlight irradiation. *Environ. Sci. Pollut. Res.* **30**, 57076–57085 (2023).
28. Davarazar, M. *et al.* Activation of persulfate using copper oxide nanoparticles for the degradation of Rhodamine B containing effluents: Degradation efficiency and ecotoxicological studies. *Chem. Eng. J.* **453**, 139799 (2023).
29. Akter, J., Hanif, M. A., Islam, M. A., Sapkota, K. P. & Hahn, J. R. Selective growth of Ti$^{3+}$/TiO$_2$/CNT and Ti$^{3+}$/TiO$_2$/C nanocomposite for enhanced visible-light utilization to degrade organic pollutants by lowering TiO$_2$-bandgap. *Sci. Rep.* **11**, 9490 (2021).
30. Zhang, Y. *et al.* Construction of TiO$_2$/Ag$_3$PO$_4$ nanojunctions on carbon fiber cloth for photocatalytically removing various organic pollutants in static or flowing wastewater. *J. Colloid Interface Sci.* **571**, 213–221 (2020).
31. Kumar, I., Mondal, M., Meyappan, V. & Sakthivel, N. Green one-pot synthesis of gold nanoparticles using *Sansevieria roxburghiana* leaf extract for the catalytic degradation of toxic organic pollutants. *Mater. Res. Bull.* **117**, 18–27 (2019).

32. Sharifi, A. *et al.* Investigation of photocatalytic behavior of modified ZnS: Mn/MWCNTs nanocomposite for organic pollutants effective photodegradation. *J. Environ. Manag.* **247**, 624–632 (2019).
33. Chahal, S. *et al.* Enhanced photocatalytic degradation of organic dye by $CeO_2$/CNT/GO hybrid nanocomposites under UV light for wastewater treatment. *Environ. Sci. Pollut. Res.* **30**, 124964–124975 (2023).
34. Altowyan, A. S. *et al.* Removal of methylene blue dye from aqueous solution using carbon nanotubes decorated by nickel oxide nanoparticles via pulsed laser ablation method. *Radiat. Phys. Chem.* **198**, 110268 (2022).
35. Al-Musawi, T. J., Rajiv, P., Mengelizadeh, N., Arghavan, F. S. & Balarak, D. Photocatalytic efficiency of $CuNiFe_2O_4$ nanoparticles loaded on multi-walled carbon nanotubes as a novel photocatalyst for ampicillin degradation. *J. Mol. Liq.* **337**, 116470 (2021).
36. Liu, S. *et al.* Anchoring $Fe_3O_4$ nanoparticles on carbon nanotubes for microwave-induced catalytic degradation of antibiotics. *ACS Appl. Mater. Interfaces* **10**, 29467–29475 (2018).
37. Pattanayak, B. *et al.* Role of precursors mixing sequence on the properties of $CoMn_2O_4$ cathode materials and their application in pseudocapacitor. *Sci. Rep.* **9**, 16852 (2019).
38. Al-Musawi, T. J., Mengelizadeh, N., Ganji, F., Wang, C. & Balarak, D. Preparation of multi-walled carbon nanotubes coated with $CoFe_2O_4$ nanoparticles and their adsorption performance for bisphenol A compound. *Adv. Powder Technol.* **33**, 103438 (2022).
39. Sandosh, T. A. & Simi, A. Morphology controlled synthesis of one-dimensional $CoMn_2O_4$ nanorods for high-performance super-capacitor electrode application. *Chem. Pap.* **75**, 2295–2304 (2021).
40. Vigneshwaran, P. *et al.* A study on the synthesis and characterization of $CoMn_2O_4$ electrode material for supercapacitor applications. *J. Mater. Sci. Mater. Electron.* **27**, 4653–4658 (2016).
41. Lu, Y. *et al.* Impacts of soil and water pollution on food safety and health risks in China. *Environ. Int.* **77**, 5–15 (2015).
42. Gao, Y. *et al.* Activity trends and mechanisms in peroxymonosulfate-assisted catalytic production of singlet oxygen over atomic metal–N–C catalysts. *Angew. Chem. Int. Ed.* **60**, 22513–22521 (2021).
43. Shah, N. S. *et al.* Hydroxyl and sulfate radical mediated degradation of ciprofloxacin using nano zerovalent manganese catalyzed $S_2O_8^{2-}$. *Chem. Eng. J.* **356**, 199–209 (2019).
44. Yao, Y. *et al.* Sulfate radicals induced from peroxymonosulfate by cobalt manganese oxides ($Co_xMn_{3-x}O_4$) for Fenton-like reaction in water. *J. Hazard. Mater.* **296**, 128–137 (2015).
45. Chen, Z., Bi, S., Zhao, G., Chen, Y. & Hu, Y. Enhanced degradation of triclosan by cobalt manganese spinel-type oxide activated peroxymonosulfate oxidation process via sulfate radicals and singlet oxygen: Mechanisms and intermediates identification. *Sci. Total Environ.* **711**, 134715 (2020).

## Acknowledgements

## Author contributions

Ayda Farajollahi: Data curation, Investigation, and Writing-original draft. Ahmad Poursattar Marjani: Project administration, Supervision, Investigation, Writing-review & editing.

## Competing interests

The authors declare no competing interests.

## Additional information

**Correspondence** and requests for materials should be addressed to A.P.M.

**Reprints and permissions information** is available at www.nature.com/reprints.

**Publisher's note** Springer Nature remains neutral with regard to jurisdictional claims in published maps and institutional affiliations.